ETH zürich

Trapped Ion Quantum Information Group

Master Thesis

Research report

Design of a calcium 2D-MOT as a cold atom source

Supervised by:

Prof.Dr. Jonathan Home

Dr.Carmelo Mordini

Dr. Henry Fernandes Passagem

EZZO Youssef 16-815-441
Group: TIQI

April 2022

Contents

List of Figures

List of Tables

Acknowledgement

First of all, I would like to thank Dr. Carmelo Mordini and Dr. Henry Fernandes Passagem who supervised me all along this project. They dedicated a lot of time and effort to familiarize me with atom trapping and quantum information research in general. They also provided me with valuable direction for laboratory work and knowledge. Many thanks also for proofreading my thesis and providing helpful feedback.

Equally I want to thank Prof. Dr. Jonathan Home, Dr. Daniel Kienzler and all the members of TIQI group for the opportunity to do my master thesis on this interesting topic.
Especially, I would like to thank Alfredo Ricci, Wojciech Adamczyk and Silvan Koch for their time and help in but not only :teaching about the various optical setups, orientation around the lab and cleaning of the setup.

Of course, I am forever thankful to my family for their constant support through everything I do.

1 Introduction

The potential of Quantum Computers (QCs) is getting increasing recognition every day. There has been a total of 2,403 papers published in Europe on the subject since 2010 [1]. One of the anticipated types of QCs is the ion-based prototype. It relies on using ions confined in space as qubits and interprets specific interactions among them as operations.

However, the methods used to trap these ions face several challenges. Ion traps aim at confining many interacting particles simultaneously to use them as entangled qubits, and methods coming from cold atoms techniques can help increase the loading efficiency. Indeed, the atoms are trapped by means of laser beams slightly shifted from the excitation frequency and a magnetic field (Magneto-Optical Traps), then they are ionised to be used as qubits. This method becomes harder to operate when one seeks to confine multiple atoms next to each other. Our work here focuses on tackling this issue by exploring the atoms' more controlled loading method into the MOT. Usually, the atoms are loaded using an oven where a beam of hot particles is directly sent to the ion traps where they will be ionised and trapped. This presents some disadvantages. It pollutes the vacuum around the trapping region, making loading even more complicated since fast incoming particles can kick out the already trapped ones. Furthermore, when loading is over, it creates an atmosphere of particles around the trap that limits the particle's lifetime. .

On the other hand, using a cold atoms source could solve some of the above-mentioned problems. Indeed, using a 2D-MOT for loading atoms will allow for a controlled amount of cold particles that can then be directed accurately by a push beam, which would make for a better loading method. Furthermore, is it a flexible source of neutral particles: be used for more controlled loading of a 3D MOT that uses neutral atoms in its experiments as intended for our loading method. It could also be used for experiments using ions to deliver neutral atoms to the trap and then ionise them to be used in quantum computing applications.

Hence, we will present this solution in the thesis. Firstly, by presenting a mathematical explanation of the MOT and the general design of the trap. Afterwards, we will turn into the specifics of the required laser setup, followed by a presentation of the chamber design, expected functioning and components. Finally, the testing results for this setup will be presented.

2 General description and design

2.1 Mathematical description

The physical effects taking place in the MOT come from laser-atom interaction. They use pressure radiation and magnetic field gradient to decelerate the atoms and confine them. It can be divided into three parts:

1. Doppler cooling beams
2. effect of the magnetic field
3. Zeeman slowing beam

As those points are general for any used atoms in MOT, we will then present the specifics of our chosen design and the choice of Calcium atoms.

2.1.1 Doppler cooling

In order to be able to confine an atom in a finite space, the first step is to use the Doppler effect by shifting the cooling lasers to the red of the resonant frequency for an atom at rest, hence exciting it and exchanging momentum with the beam only when the atom is propagating towards the beam at a given velocity.
More rigorously, first, we consider a quantized atom described by its energy levels interacting with a laser beam described by a classical electrical field of well-defined frequency. The laser beam is driven by a single frequency, and only two energy levels are considered for the atom. In a semi-classical picture, the force on an atom is given by [2], Page 30 :

$$\mathrm{F} = \left\langle \frac{\partial \hat{\mathcal{H}}}{\partial \mathrm{z}} \right\rangle \tag{1}$$

Where the z-axis here is the propagation axis of the laser beam, the interaction Hamiltonian considered here has the following expression:

$$\hat{\mathcal{H}} = -e\vec{\mathrm{E}}(\vec{\mathrm{r}},\mathrm{t})\vec{\mathrm{r}} \tag{2}$$

Such that $\vec{E}(\vec{r},t)$ describes the electrical field of the laser beam and $\vec{r}$ the position of the atom's valence electron. Here in this simple picture we consider the photon to be traveling in the positive z-direction, then the electric field can be expressed as:

$$\overrightarrow{E}(\vec{r},t) = E_0\hat{\varepsilon}\cos\left(kz-\omega_\ell t\right) \tag{3}$$

where $\hat{\varepsilon}$ is the unit polarization vector, ω_ℓ is the laser frequency and E_0 is the amplitude of the light field. The coupling Hamiltonian is then written as $\mathcal{H}(t) = \hbar\Omega\cos(kz - \omega_\ell t)$, where Ω is the Rabi frequency defined as :

$$\Omega \equiv \frac{-eE_0}{\hbar}\langle e|r|g\rangle \tag{4}$$

and its derivative is:

$$\frac{\partial\Omega}{\partial \mathrm{z}} = (\mathrm{q_r} + \mathrm{iq_i})\,\Omega \tag{5}$$

Where:

$$\begin{aligned} \mathrm{q_r} &= \mathrm{Re}\left(\frac{1}{\Omega}\frac{\partial\Omega}{\partial \mathrm{z}}\right) \\ \mathrm{q_i} &= \mathrm{Im}\left(\frac{1}{\Omega}\frac{\partial\Omega}{\partial \mathrm{z}}\right) \end{aligned} \tag{6}$$

Furthermore for an expectation value of $\mathcal{A}$ we have $\langle\mathcal{A}\rangle = \mathrm{Tr}(\rho\mathcal{A})$ Hence the following expression of F:

$$F = h\left(\frac{\partial\Omega}{\partial z}\rho_{eg}^* + \frac{\partial\Omega^*}{\partial z}\rho_{eg}\right) \tag{7}$$

Deriving this result requires the RWA (Rotating wave approximation) that consists of neglecting terms oscillating with the laser frequency. Note that the force depends on the optical coherence between the ground and excited states, ρ_{eg}. By using the expressions given by eq.(1.6), the force is rewritten as:

$$F = \hbar q_r\left(\Omega\rho_{eg}^* + \Omega^*\rho_{eg}\right) + i\hbar q_i\left(\Omega\rho_{eg}^* - \Omega^*\rho_{eg}\right) \tag{8}$$

After applying the RWA the electric field can be written as:

$$\mathrm{E(z)} = \frac{\mathrm{E_0}}{2}\left(\mathrm{e^{i(kz-\omega t)}} + \mathrm{c.c}\right) \tag{9}$$

The RWA causes the positive frequency component of $E(z)$ to drop out by calculations with the expressions given above. Then the gradient of the Rabi frequency becomes proportional to the gradient of the surviving negative frequency component, so that $q_r = 0$ and $q_i = k$. For such a travelling wave, the amplitude is constant, but the phase is not, and this leads to the non-zero value of q_i. By reference of [2] using the solution of the optical Bloch equations gives:

$$\rho_{\mathrm{eg}} = \frac{\mathrm{i}\Omega}{2(\gamma/2 - \mathrm{i}\delta)(1+\mathrm{s})} \tag{10}$$

This finally gives

$$\mathrm{F} = \frac{\hbar \mathrm{s}}{1+\mathrm{s}}\left(-\delta \mathrm{q_r} + 1/2\gamma \mathrm{q_i}\right) \tag{11}$$

The detuning δ is

$$\delta = \omega_\ell - \omega_\mathrm{A} \tag{12}$$

With ω_A the atomic transition frequency and ω_ℓ the laser frequency. And the decay rate γ is defined as

$$\gamma = \frac{1}{\tau} \tag{13}$$

Such that τ is the lifetime of the excited state. Eq. (11) can be described as two distinct forces, the scattering force (imaginary part) and the dipole force (real part).

The scattering force of a photon-atom spontaneous emission cycle corresponds to the momentum absorbed and emitted by an atom.

$$\mathrm{F_s} = \hbar \mathrm{k} \gamma \rho_\mathrm{ee} \tag{14}$$

where ρ_{ee} is the excited state population defined by the optical Bloch equations. Therefore, by calculating Eq. (1.14), the scattering force is

$$\mathrm{F_{sp}} = \frac{\hbar \mathrm{k} \gamma}{2} \frac{\mathrm{s_0}}{1+\mathrm{s_0}+(2\delta/\gamma)^2} \tag{15}$$

The saturation parameter s_0 is

$$\mathrm{s_0} = \frac{\mathrm{I}}{\mathrm{I_0}} \tag{16}$$

where $\mathrm{I_0} = \frac{2\pi^2 hc\Gamma}{3\lambda^3}$ is the saturation intensity and I is the intensity of the laser the expression is obtained from [3].

The second force term comes from the polarization of the light changes within a standing wave. Composed of two counter-propagating beams, this results in a spatially modulated light shift which produces a dipole force. It is important to note that this force is not manifested for our case of a travelling wave since the real part is equal to 0. For completeness, we will still discuss it briefly; it has been derived in [2], P. 33 with the expression:

$$\mathrm{F_d} = \frac{2\hbar k \delta s_0 \sin(2kz)}{1+4s_0\cos^2(kz)+(2\delta/\gamma)^2} \tag{17}$$

for atoms with nuclear spin, a combination of dipole and scattering forces coming from spatial gradients of the polarisation is the mechanism behind sub-doppler cooling. It is a cooling effect that allows achieving temperatures for particles lower than the Doppler cooling limit, which is the standard limit of the MOT. We will further see that the calcium isotope used has no nuclear spin, and hence no sub-doppler cooling is possible. Further more, in cases of high saturation i.e. $\mathrm{s}_0 \gg 1$, F_s can be expressed as :

$$\mathrm{F_{sp}} = \frac{\hbar \mathrm{k}\gamma}{2} \tag{18}$$

If the intensity gets higher the ratio of stimulated emission to spontaneous emission gets higher. Hence, stimulated emission does not cause "cooling" as it is directed along the absorbed beam direction. Instead, it is used to trap neutral atoms in optical traps or optical lattices.

Notably, the results shown above are for the simple case of an atom at rest still, considering that the atom is moving in space will result in considering the Doppler effect in the equations. This, as shown in [3] will result in adding a term to the detuning δ. Indeed, an atom moving with velocity v in the direction of propagation of the laser will perceive the laser frequency Doppler-shifted down by $2\pi v/\lambda = kv$, for an overall detuning now of $\delta - kv$.

Furthermore, in the case of the MOT the beam on one axis is incoming from both directions. This will result in two scattering forces to be considered from opposite sides their modified expression due to the doppler effect will be:

$$\mathrm{F}_{s\pm} = \pm \frac{\hbar \mathrm{k}\gamma}{2} \frac{\mathrm{s}_0}{1 + \mathrm{s}_0 + (2(\delta \mp \mathrm{kv})/\gamma)^2} \tag{19}$$

The addition of the two forces becomes the new total scattering force $F_s = F_{s+} + F_{s-}$ In order to better illustrate how these forces would affect the velocity of the atom in [**?**] the assumption that $s_0 \ll 1$ gives the following expression for the full scattering force:

$$F = s_0 \frac{\hbar k \gamma}{2} \frac{kv}{\gamma} \frac{16\delta/\gamma}{1 + \frac{8}{\gamma^2}\left(\delta^2 + k^2 v^2\right) + \frac{16}{\gamma^4}\left(\delta^2 - k^2 v^2\right)^2} \tag{20}$$

From this expression we want to be able to observe more clearly the realtion of velocity to Force. Hence, we set $\delta = -\gamma/2$ this gives the following graph :

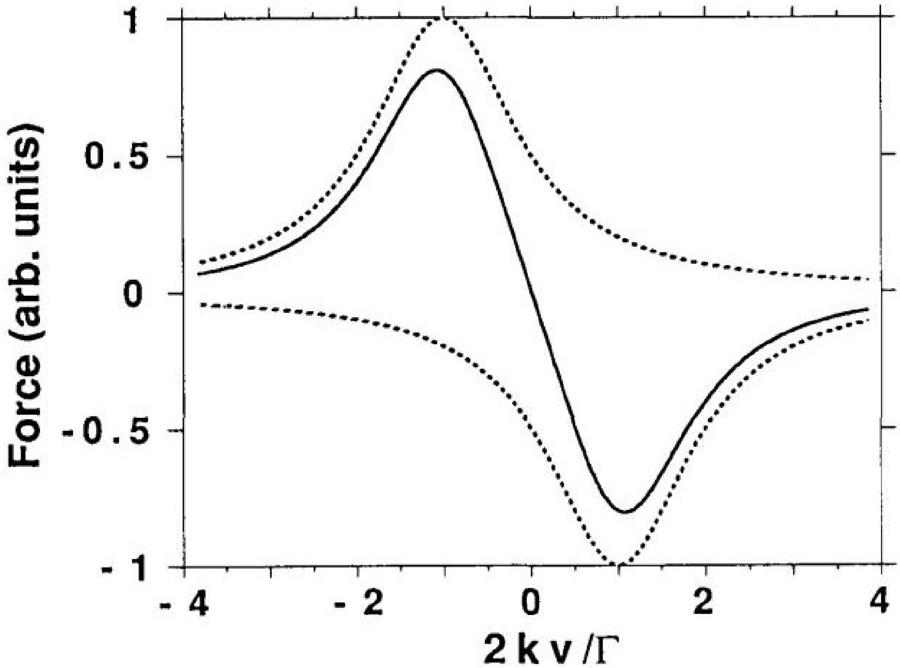

Figure 1: *Forces in function of velocity (times the $2k/\gamma$ term) in arbitrary units from [3], The dashed curves represent the individual forces due to the two counter-propagating beams, and the solid curve is the net force*

We can note the linear region near v=0, and the form of the graph implies that if the atom gains velocity towards one of the photon directions, it will experience a repulsive force. Furthermore, we note that when the atom changes direction, the force consequently changes sign, Hence having a force directed opposite to the velocity vector. Mathematically, this means the force acts as a damping force linearly with velocity (i.e. $F = -\alpha v$) where α is defined as follows from :

$$\alpha = 4\hbar k^2 s_0 \frac{2\delta/\gamma}{(1 + 2\delta/\gamma)^2} \tag{21}$$

The critical velocity $v_c \approx \pm\delta/k$ is the velocities above which this approximate linear relation to velocity is no longer valid, and the Doppler cooling is no longer efficient.

This is the first important principle to fully understand how the MOT manages to confine an atom in space.

2.1.2 effect of the magnetic field

The magnetic effects in the MOT are generated by a quadrupole-like magnetic field, and the optical effects are represented by the two counter-propagating beams on each axis. They constitute the base design for a magneto-optical trap (MOT). As we showed previously, the system uses optical cycling, which excites the atom and then de-excites it with a resulting change of momentum direction.
To explain the reason for adding a magnetic field in addition to the laser beams, one can take a deeper look into the total detuning. Indeed, the atom in motion needs this detuning to be equal to 0 in order to be excited and reverse its direction. Hence the velocity needs to satisfy the relation:

$$kv = \omega_\ell - \omega_A \tag{22}$$

By adding the magnetic field, the velocity becomes bound by an upper limit which is the capture velocity as shown in [4]. The capture velocity is the maximum velocity of an atom while entering the trap (inside the magnetic field and the beam paths) and can be captured. This differs from escape velocity, which defines the maximum velocity that an atom can have at the trap centre.In the reference the relation is given by $v_{\mathrm{es}} \cong 0.7v_{\mathrm{c}}$. Indeed the Magnetic field causes a Zeeman shift in the excitation frequency of the atom with expression:

$$\delta_{\mathrm{zeeman}} = \pm\mu \mathrm{B}/\hbar \tag{23}$$

Such that μ is the effective magnetic moment, this changes the total shift and the scattering Force to have the following expressions:

$$\delta_{\pm} = (\omega_\ell - \omega_A) \mp kv \pm \mu \mathrm{B}/\hbar \tag{24}$$

$$\mathrm{F}_{\pm} = \pm\frac{\hbar \mathrm{k}\gamma}{2}\frac{\mathrm{s}_0}{1 + \mathrm{s}_0 + (2\delta_{\pm}/\gamma)^2} \tag{25}$$

The Magnetic field B felt by the particle depends on its position, affecting the Zeeman split into energy levels. This is shown in [2] in the following graph:

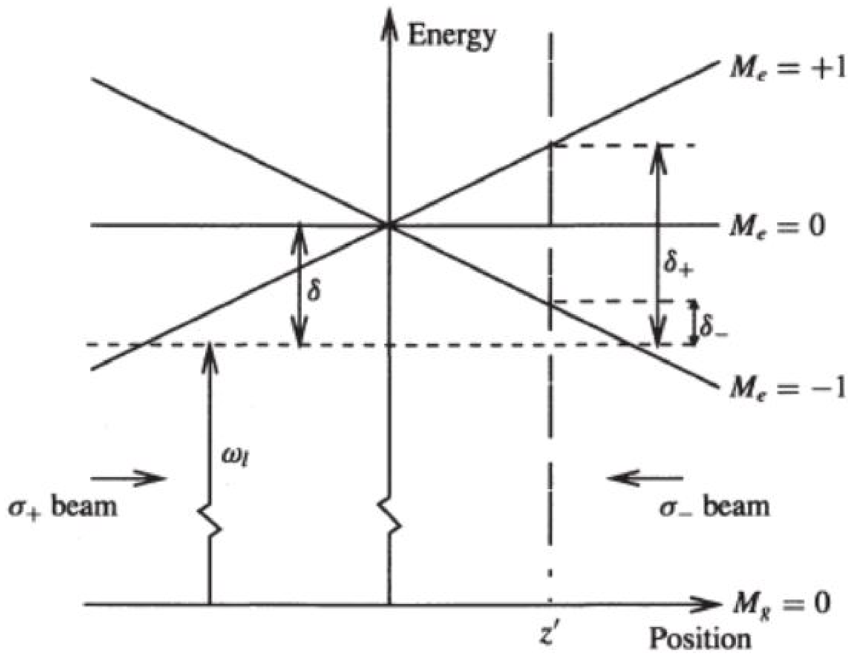

centring

Figure 2: *the qualitative representation of energy levels of an atom in function of position in a quadrupolar magnetic field where the field is null at z=0 (1D)*

Here the ground state is denoted M_g and te excited sub-states M_e. The black dotted line shows the energy of the photon with frequency ω_l detuned by δ from $\mathrm{M}_l = 0.\sigma^+$ and σ^- represent the polarisation of the incoming positively and negatively circular-polarised beams. $\delta_+$and δ_-describe the detuning from the frequency of the laser beams to the $\mathrm{M}_e = +1$ and $\mathrm{M}_e = -1$ magnetic sub-levels. The atoms further from the magnetic quadrupole null experience larger Zeeman shifts, resulting in a smaller effective laser detuning $\delta_-$and an increased scattering rate. The laser directions ensure that the two scattering forces always act towards the centre. The dependency of detuning on the position via the magnetic field acting as the confining effect in space, along with the constraining on velocity by the Doppler shift being the cooling factor on the atoms, is what makes the trapping of the atoms possible and is the functioning principle of Magneto-Optical traps.

2.1.3 Zeeman slowing beam

Now that we have shown in theory how the MOT would be able to function, there is a remaining parameter that needs to be controlled, the Capture velocity. Indeed, since the atoms' flux will be relatively hot (implying high velocity), they need to be cooled down and slowed such they do not surpass the capture velocity of our MOT. Later in the design section, it will be shown why the atom will be coming with a high velocity. The proposed solution is to attach opposingly to the atom flux a Zeeman slowing beam. This beam will be characterised by a higher redshift in frequency from the excitation level than the Doppler beams, such that it does not reverse the particles' momenta entirely but only slow it down (or cool it). This statistically is expected to show a much better capturing efficiency for our MOT, as shown in [4], where the loading rate of atom/second has increased from a 10^8 scale to 10^9.

Zeeman slowing requires the presence of a magnetic field gradient and uses the shift in resonance due to the Zeemann shift as shown in eq.24 this creates a broader range for the Doppler cooling to take place; hence it tackles the issue of narrow resonance of atoms for Doppler cooling in the MOT light beams. This slowing method is convenient in our work frame since a field gradient is present for the MOT.

Conveniently, the MOT provides a magnetic quadrupole in a trapping region. By designing the trap such that there is also a magnetic field in the direction of the atomic beam from the atom source. It can be exploited to make a Zeeman slower together with an extra light beam facing the source. This would make for a compact design as it avoids adding another magnet for this slowing method [15].

2.2 Main components of the design and requirements

As we have shown the functioning principles of our setup, it is important to focus on what components will be needed to provide the desired conditions for the success of our setup. This can be divided into two parts that will be later detailed in full: the laser setup and the MOT chamber.

2.2.1 Requirements of the laser setup

In practice, the final purpose of the setup is to build a 2D MOT as an atom source for a 3D MOT, which will be the first step of a cold atoms experiment. This, in terms of the laser setup, will require four beams in total. Two Doppler cooling beams for the 2D-MOT, one Zeeman slowing beam and an additional push beam to transport the atom into the 3D-MOT. All these beams will need to be controlled both in frequency and amplitude, as shown in Chapter 3. It is important to note that we only use the first three beams for the work conducted here. Nevertheless, for completeness, we will also show the setup of the push beam

2.2.2 Requirements for the MOT chamber

The MOT chamber has to hold several components together. Hence it needs several entries points all suited for each component. First, it needs an adapted connection to the Calcium atom oven that will be the source of atoms. Second, it will require adapted connections for the Doppler beams and their reflectors on their opposite side. Thirdly, an entry point for a vacuum pump ensures that the chamber does not have particles that might interfere with atom flux and the trap. Furthermore, the magnetic placements for the trap need to be symmetric and robust to avoid variations in the magnetic fields. Finally, The Zeeman slowing beam must be facing directed to the oven without facing it directly to avoid covering the viewport in front of the beam.

All these points need to be taken into account such that in the 2D-MOT: the atoms are confined in the plane of the laser beams, There is no force acting on the atom other than the beams scattering forces, and the only contribution to the velocity on the axis comes from spontaneous emissions. Furthermore, a UHV pressure (between $10^{-9} and 10^{-10}$ mbar) is needed since, at high pressures, the atom-atom interaction rate exceeds the photon-atom interaction rate, and the MOT will not function properly.

2.3 Calcium atoms specifics

Vapour pressure For a hydrogen atom (corresponding to the two-level model presented before), the allowed electronic transitions are governed by the presence of one electron. Calcium is classified as an Alkali earth element with two valence electrons. This motivates us to present the physical properties of calcium that would interest us.

2.3.1 Physical properties of calcium

Calcium is an Alkaline earth element with a melting point at 840°C and boils at 1480°C [5]. Furthermore, another essential property is the vapour pressure. This is the pressure of a vapour in equilibrium with its solid and liquid phases, and it is a measure of how many atoms are released from a solid as it is heated. This will be important for our Calcium atom flux, as it will be released from a heated oven, allowing us to know how much heat is needed to release the Calcium atom from its solid form. The vapour pressure in general can be modeled with the equation:

$$\log_{10} P = 5.006 + a + \frac{b}{T} + (c * \log_{10} T) \tag{26}$$

Such that P is the vapour pressure in mPa, and a,b and c for Calcium take the values: a=10.127, b=-9517 and c=-1.4030 [6]. Finally, T is temperature measured in Kelvin. In figs. 3 and 4, the different temperatures to attain similar vapour pressures for Calcium and and Potassium, an alkali metal, are shown:

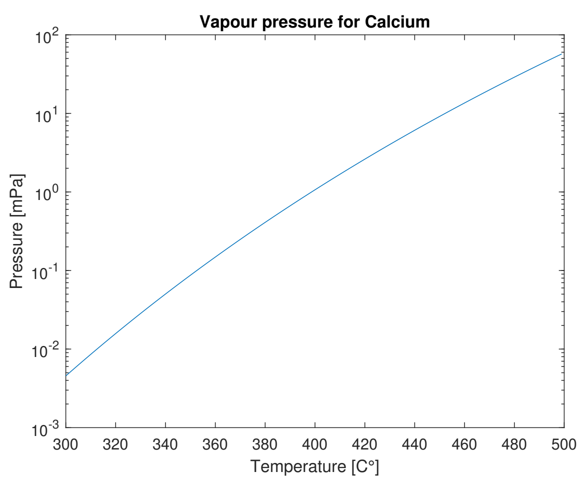

Figure 3: Vapour pressure in function of Temperature for Calcium

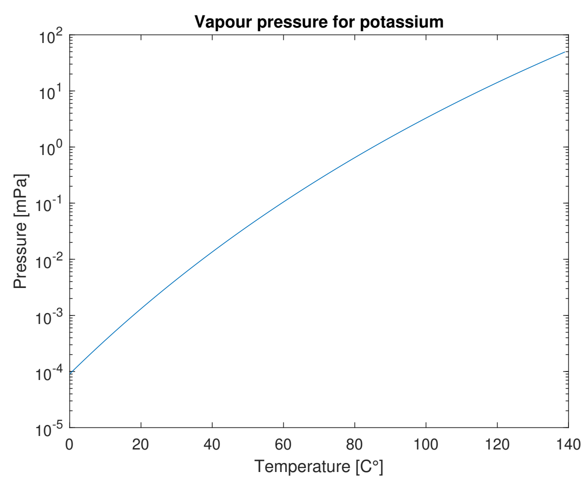

Figure 4: Vapour pressure in function of Temperature for Potassium

The exact values for the vapour pressure of these metals [6], show that to achieve a similar vapour pressure, a much higher temperature is needed for calcium.

Properties of the Calcium atom The Calcium atom used in our experiment is the ^{40}Ca isotope which accounts for 97% of Calcium on earth [7]. The first feature of this isotope is that by looking at the total angular momentum of the ground state :

$$1s^2 2s^2 2p^6 3s^2 3p^6 4s^2 \quad {}^1\,\mathrm{S}_0 \tag{27}$$

This has no hyperfine structure for the ground state; hence there is no nuclear spin. Furthermore, the isotope has two valence electrons which result in singlet and triplet energy level schemes, respectively. From the data presented in [10] we can see in relevant energy levels for the work described in the thesis:

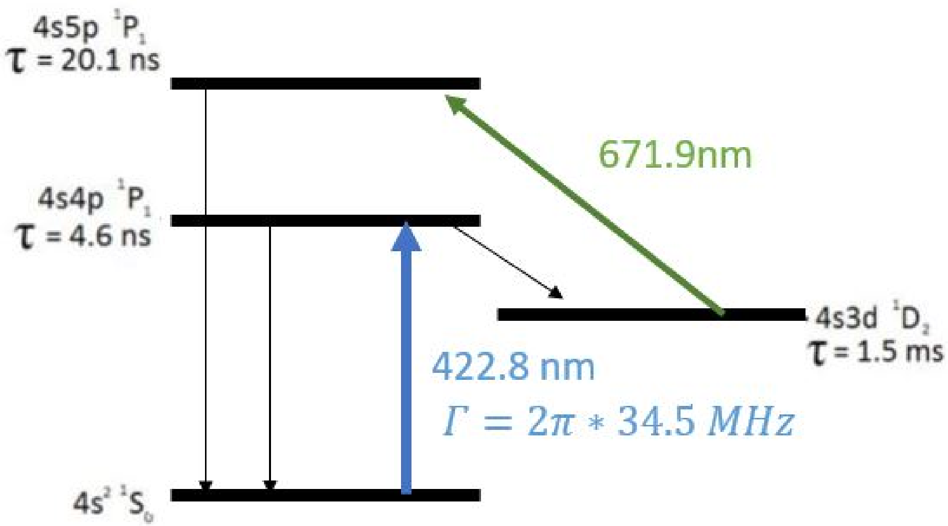

Figure 5: *Relevant energy levels of* ^{40} *Ca, lifetime note the cooling and trapping line at* 423 nm *with its' linewidth and the repumping laser at* 671 nm *(not discussed in-depth here).*

The $^1S_0 - {}^1P_1$ transition is the one used here for laser cooling. This is due to the short upper-state lifetime of the $^1P_1$ level makes it ideal for laser cooling since a shorter absorption-emission cycle increases the scattering force. The other energy levels are interesting when we try to use the Ca atom as a qubit since we are trying to achieve a long coherence time and are interesting in decay levels and repumping. In the case of this MOT, the atoms are not yet utilised as a qubit.

These past points show the general constraints that need to be considered while designing, building and testing our setup.

3 Laser setup

This section will present and analyse the laser setup that we designed. This setup aims to provide all the different laser beams needed for the MOT.

3.1 Design and outlay

In our setup there is 4 beams in total required for the 2D-MOT to function properly. Hence, the following design was proposed in order to be able to achieve each of those beams requirements:

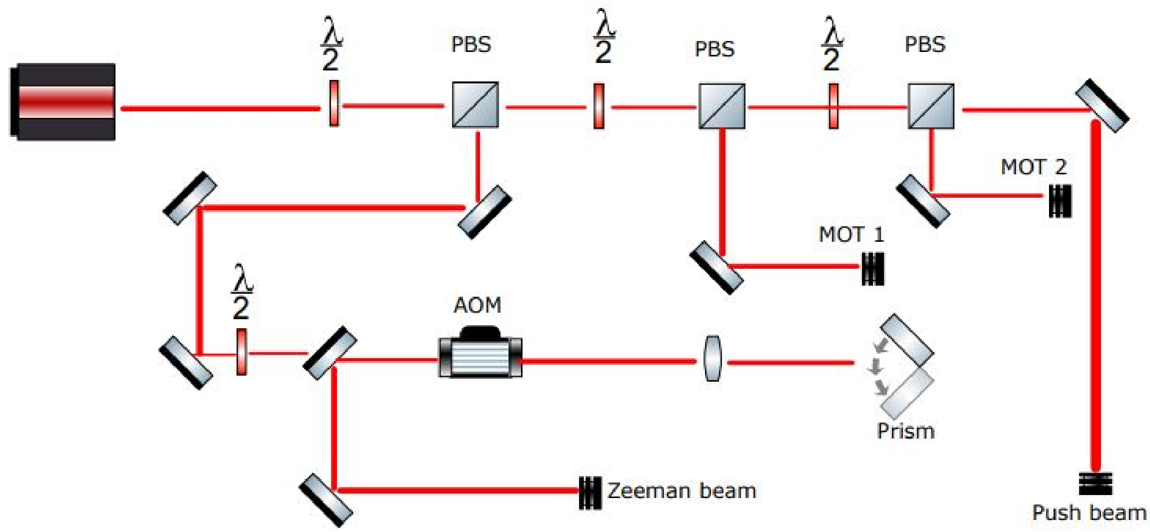

Figure 6: *Design of the laser system*

First, the laser source needs to provide a light at 423 nm with enough power for all the required beams. We use a Diode laser as a light source for the system's initial setup and connect to our setup through fibre. Secondly, there are several half-waveplates followed by polarizing beam splitters (PBS). The combination of the two allows the splitting of the beam in two whilst controlling the power ratio between these two outgoing beams via the rotation of the waveplate. Thirdly, The mirrors are used to control the direction of the beam, which is useful for a more compact setup and for aligning the beams into the collimators. Finally, the Zeeman slowing beam setup and where they will be connected to our MOT chamber.

In the following parts, parts of the setup will be discussed in-depth, where we will try to justify or design of choice for each of them.

3.2 Laser source

We first use a laser diode at 423 nm for our laser source, which provides us with enough power for laser alignment and for the functioning of the AOM (which will be explained later on). To use this source, several preparations had to be made. Firstly, a collimation setup needs to split part of the beam and send it into a collimator. Hence we use the following setup:

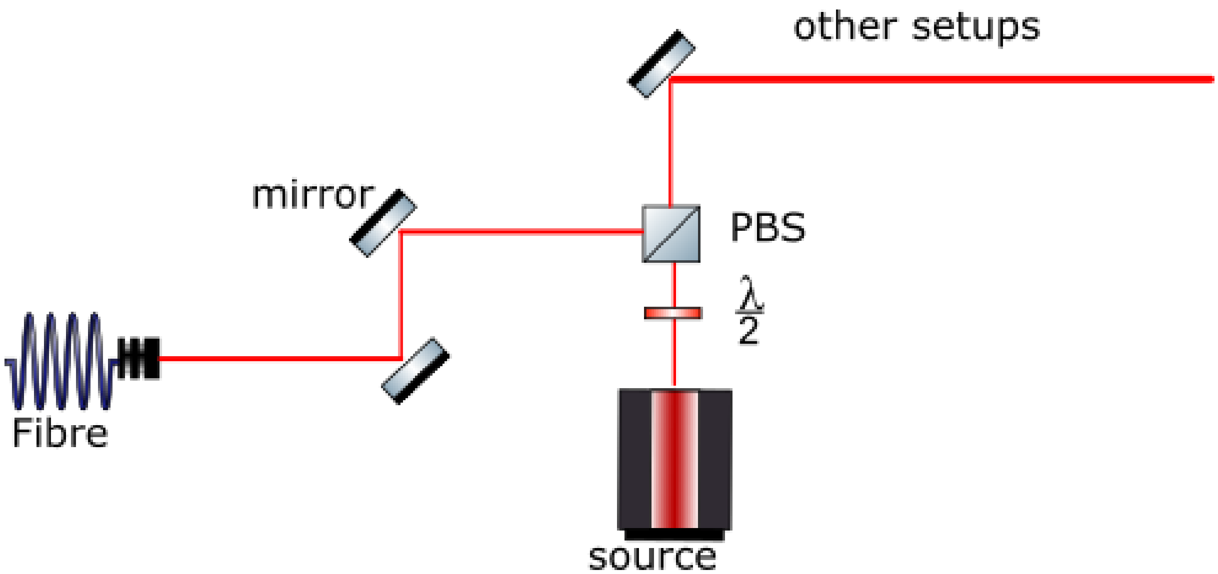

Figure 7: *setup to split the beam of the laser source to use for our setup*

A useful method to inject light into an optical fibre is to use a "laser pen", a small laser source directly attached to the other end of the fibre, and adjust the mirrors such that the outgoing beam from the laser pen follows the same path as the incoming beam from our laser source.
Secondly, a method called "beam walking" is used to maximise the efficiency of the collimator, where we carefully chance the vertical and inclination angles of two mirrors to find the optimal alignment. Indeed, the entry position and angle of the beam will affect its focussing efficiency into the fibre. This is because the laser pen has a different wavelength than our source, which will require different coordinates for the beam for maximum efficiency. The collimator used in this setup has an 8mm focal length and gave a 83% efficiency after beam alignment.

Furthermore, after connecting the optic fibre to the collimator, the light is transferred to another room via connectors between two fibres since the distance is relatively long. Afterwards, it is connected to another collimator of a focal length of 2mm since the beam width needs to be under 3.6 mm to go through the Zeeman setup without deforming the beam shape. The focalisation of the collimator makes the widening of the beam over distance minimal.

3.3 Zeeman beam setup

As previously shown, the frequency of the Zeeman slowing beam needs to be red-shifted shifted from the excitation frequency of the Calcium atom. In our experiment, we seek a shift of around 200 MHz. To do that, an Acousto-optic modulator(AOM) is used. Its basic working principle is presented in the figure below.:

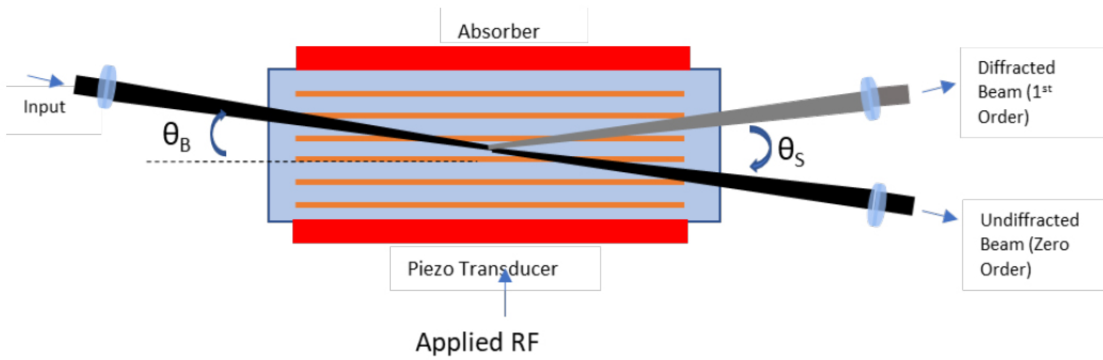

Figure 8: *Basic description of the AOM [16]*

An acousto-optic modulator consists of a piezoelectric transducer that creates sound waves in an optical crystal. An optical beam is diffracted into several orders by the vibration of the material with a sinusoidal wave and tilting the AOM. The light is reflected from the flat sound waves into what is called the "first diffraction order". The diffraction shown here is due to Bragg's law, where the incident light comes at Bragg angle $\theta_B \approx \sin\theta_B = \frac{\lambda}{2n\Lambda}$, measured perpendicularly to the propagation of the sound wave in the crystal.

In the AOM when the incident and outgoing light beams are at Bragg angle, a diffraction pattern emerges where an order of diffracted beam occurs at each angle θ_s that satisfies:

$$2\Lambda \sin\theta_s = m\frac{\lambda}{n} \tag{28}$$

Here, m takes integer values and is the order of diffraction, λ is the wavelength of light in a vacuum, n is the refractive index of the crystal material, and finally, Λ is the wavelength of the sound. This diffraction causes a shift in the frequency of the outgoing beam such that for a frequency f of the light beam and F for the sound wave, we have:

$$f \rightarrow f + mF \tag{29}$$

3.3.1 AOM model specifics

The AOM used in our setup has a peak diffraction efficiency of 100 MHz. We use the double passing configuration since we seek to achieve a 200 MHz red shift from our original frequency.

The double passing consists of passing the beam through both sides of the AOM, such that the incident beam for the second diffraction is the first-order diffracted beam from the first incident beam. This means that we perform two diffractions of m=-1 and F= 100MHz hence we have for our light frequency f :

$$f \rightarrow f - 2.(100MHz) \tag{30}$$

this is the method we use in our setup to achieve a redshift of 200 MHz.

3.3.2 setup of the double passing

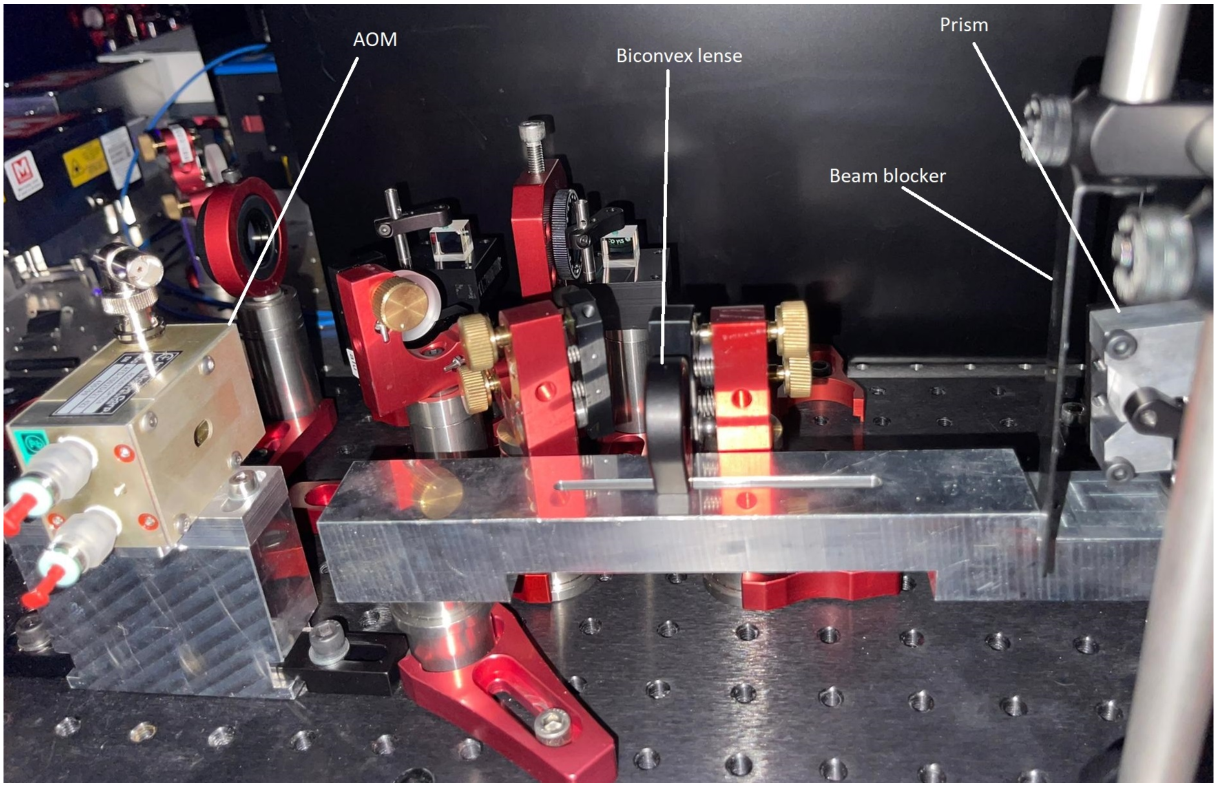

Figure 9: *setup for the Double passing*

A biconvex lens is shown after the AOM, followed by a beam block and a prism. In practice, we are trying to cause first-order diffraction through the AOM, then align it so it moves parallel to the 0th order beam. This is why the biconvex lens is used. Finally, a beam blocker will block the 0th order beam. The prism will send the 1st order beam into the opposite direction but on a more elevated plane, where it will be diffracted for a second time. Hence, it goes through the lens and the AOM without crossing with the incoming beam and affecting the polarisation, which the AOM's efficiency depends on.

3.3.3 Parameters determination

Of course, there are some parameters to be controlled to realise this setup. First off, the beam diameter, as previously mentioned, the beam diameter needs to be small enough to avoid deformation of the beam shape, which could result in efficiency losses. The collimator focal length controls this by the following equation. from [9]:

$$d \approx 4\lambda \left(\frac{f}{\pi[MFD]} \right) \tag{31}$$

Where f is the focal distance, d is the beam diameter, λ the wavelength and MFD is the mode field diameter which describes the width of this intensity profile for our beam. From the datasheet, we have that for the CFC-2X-A collimator model (f=2mm, MFD=3.3µm) and $\lambda = 423nm$, the beam width becomes approximately 1mm. This will be a small enough diameter for our AOM opening.

On the other hand, the distance between the biconvex lens and the AOM needs to be long enough for the 0th and 1st order beams to be differentiable, i.e. the distance between the two beams needs to be at least equal to the beam width before going through the lens as shown in the graph below:

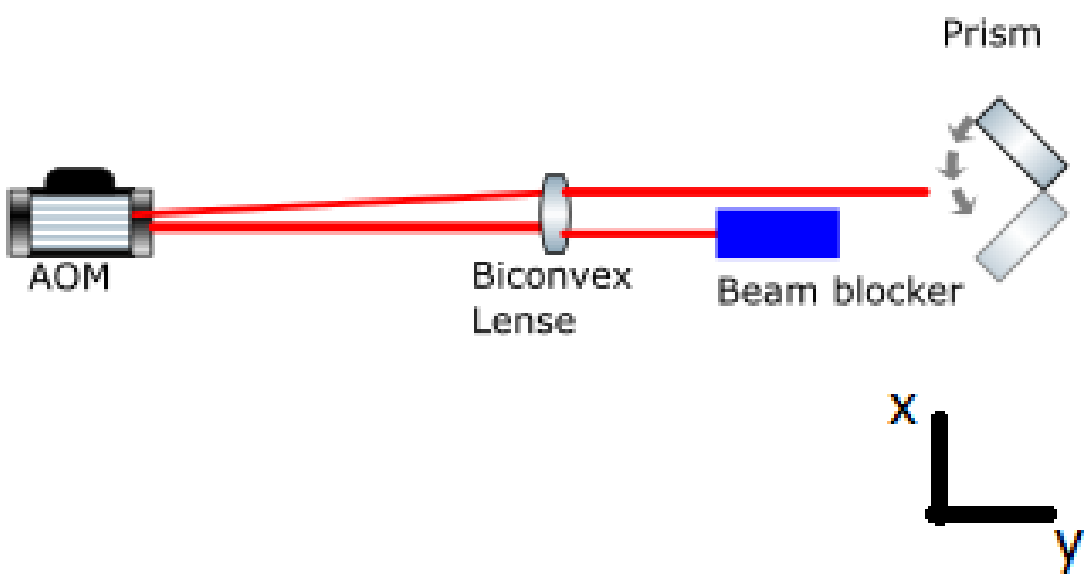

Figure 10: *Beam paths of the 1st and 0th order beams*

After the lense, this will allow us to block the 0th order beam without causing losses to the first-order one. By supposing that the 0th order beam will be on a perpendicular path to the lense, we have that the distance L required for the two beams to be separated by d is :

$$L = \frac{d}{tan(\theta_s)} \tag{32}$$

Furthermore, from Eq.28, we can identify the value of the angle θ_s. For a sound frequency at 100 MHz, we have a wavelength of approximately 45400 nm. This results in an angle of approximately 3.2 millirad. This results in a minimal distance of 1.7 cm before the two beams are distinguishable. With the focal distance of the lense being 12.5 cm, it is safe to assume that the beams will be differentiable even if the diameter is widening due to the travel distance.

Prism placement and collection of the beam Finally, it is important to mention that the second diffracted beam collected will be incident from the prism will be on a higher plane than the rest of the laser path; hence when going through the lens again and crossing the AOM, it will be possible to collect it via a mirror from a lower height as shown below:

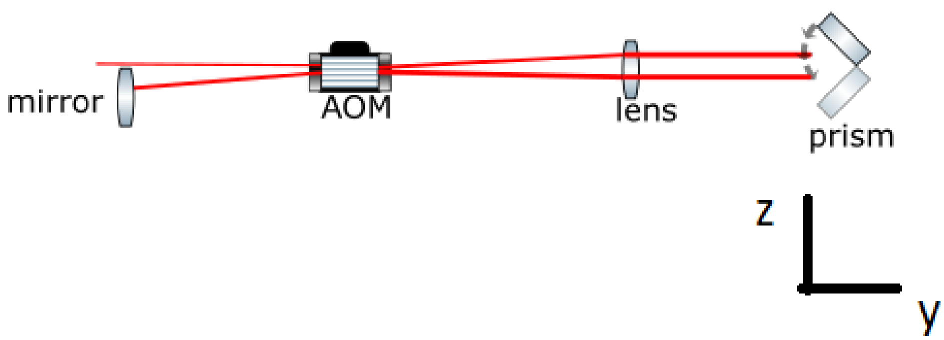

Figure 11: *1st order beams path on the y and z-axis for the AOM double passing*

It will finally go through another collimator connected to an optic fibre. This Double passing setup, along with collimation of the beam, presents a 50 % efficiency for the laser power.

3.3.4 Operating of the AOM

In order to be able to control the frequency fed to the AOM several preparations need to be made . The instruments used in order to do so are shown in the figure below:

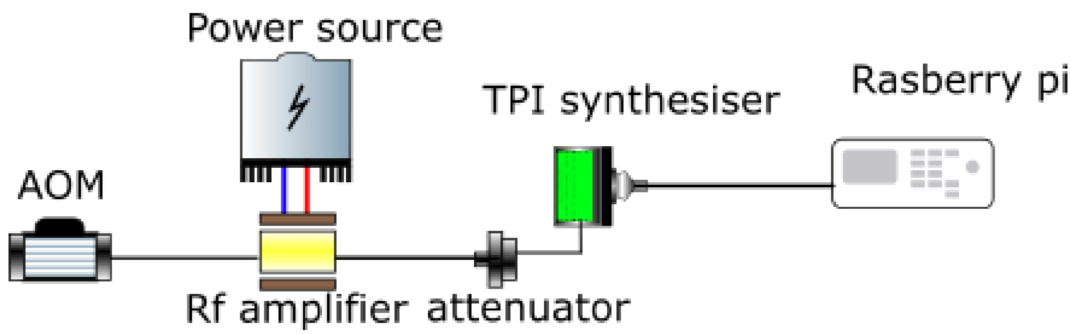

Figure 12: *Devices used for the AOM control*

Firstly, the RF frequency is set by a TPI-Synthesizer. In order to do so, the synthesiser is controlled via a Rasberry-pi device. The device used a plugin software we developed, shown in the index. This allows the user to have an interface from which to set the TPI parameters remotely as long as he is connected to the Lab network. Furthermore, the code is written such as it can be edited for different TPI models whilst still maintaining its same interface. This is specifically why we used the plugin method. Afterwards, an RF amplifier is used to achieve the optimal intensity of the sound wave required. As it has a constant amplification, it is suggested to use attenuators to fine-tune it for the optimal intensity corresponding to the AOM used. In our case, the intensity sought was 30 dB. This amplifier is powered via a power source to be fixed at 26 .4 volts (and 0.7 A). This setup and optimisation of the beam's angle allowed an 80% efficiency for each first-order diffraction in the AOM.

3.4 Current status and operating setup

The points shown before in the setup present the final product desired in terms of the push beam and the two MOT beams. Nevertheless currently, this experiment consists of developing and testing the Calcium 2D MOT. Hence, the push beam dedicated to transporting the atoms into another setup through a connection (3D MOT, for example) will not be exposed here. Concerning the two doppler beams, one will only be used and, after collimation, will be separated via a beam splitter. This allows for an equal repartition of the beam intensity between the two beams. This results in the setup used here:

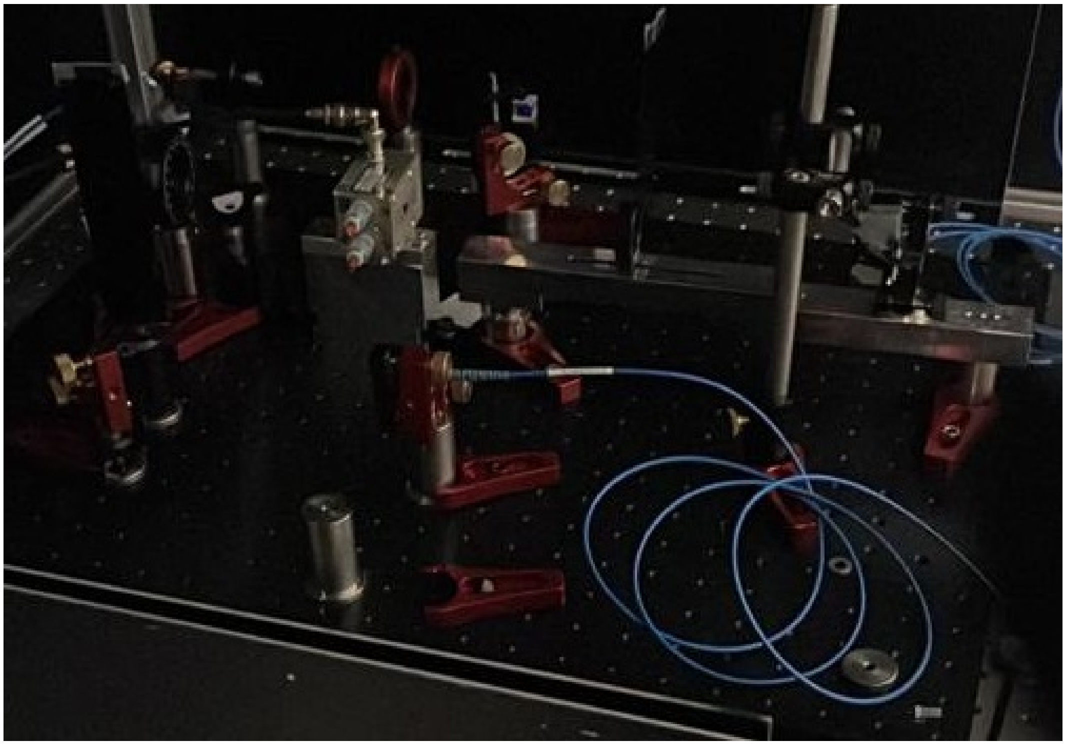

Figure 13: *Final setup for our experiment. We use only one MOT beam which is split via a beamsplitter.*

Furthermore, the laser source used for the setup that we presented whilst being very useful and practical for the first stage of our experiment. It allowed us to optimise the efficiencies with a high enough power whilst keeping the setup out of the main lab was logistically useful. Nevertheless, the setup having a relevant amount of power loss for every collimation, alignment and double passing required a more powerful laser source (around 40 mW needed) than the original Diode laser (4mw at the output of the 2mm collimator). Furthermore, in order to have Doppler beams shifted from the excitation wavelength. In terms of frequency for a 422.8 nm wavelength, the corresponding frequency is $7,09.10^5 GHz$. This means that we need a laser source where a possible control of the frequency is possible such that a 50 MHz redshift is possible.

Hence, the laser source used for the full operation of the 2D-MOT is the ti:saph laser setup. It allows for the power output required and has a user interface that allows the setting of the wavelength. Furthermore, the laser setup is moved to the main lab after optimising the efficiency at each step. This will be then connected to the MOT setup, which we will expose in the next chapter.

4 Design of the chamber

In this part, the design for the chamber of the 2D-MOT is presented. The usage and chosen design of each part of the assembly will be presented. The parts of the chamber can be divided as follows:

1. Calcium oven
2. MOT beams mounts and reflectors
3. Zeeman beam connection
4. Permanent magnets setup
5. Pumping setup

4.1 Calcium oven

4.1.1 oven mounting

As shown in fig.3 the temperatures for the vapour pressure of the calcium atom shows that our oven would need to withstand temperatures between 450 and 500 C°, since this is where the desired vapour pressure is reached. This is why the Calcium granules are held in a vessel connected to copper wires that heat the vessel directly. The vessel is suspended in the middle of a connecting tube by ceramic rods that can tolerate high temperatures. The metal rods are held at the entry port for the main chamber via a disk which also has an opening for the collimation of the particle flux. The entry of the chamber for the oven is shown in the figure below:

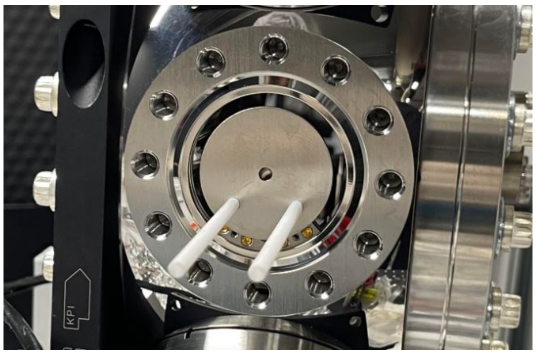

(a)

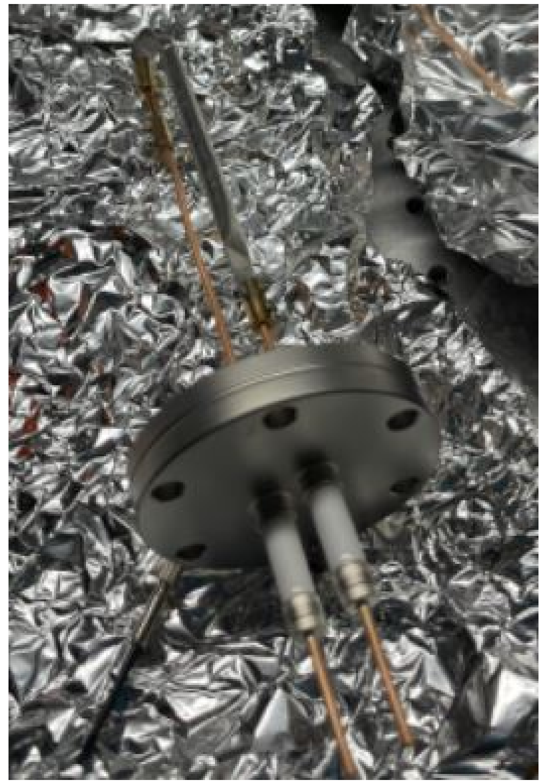

(b)

Figure 14: *Collimation disk mounted on the chamber port and the oven setup meant to be suspended on the ceramic rods attached to the disk*

The oven is sealed in a tube mounted on the chamber viewport, such that the end of the wires are on the outside whilst still the setup is isolated from the exterior. The suspension of the vessel and the wires are necessary since it allows for a better alignment of the flux into the particle collimator. The final mount of the oven is shown in the figure below:

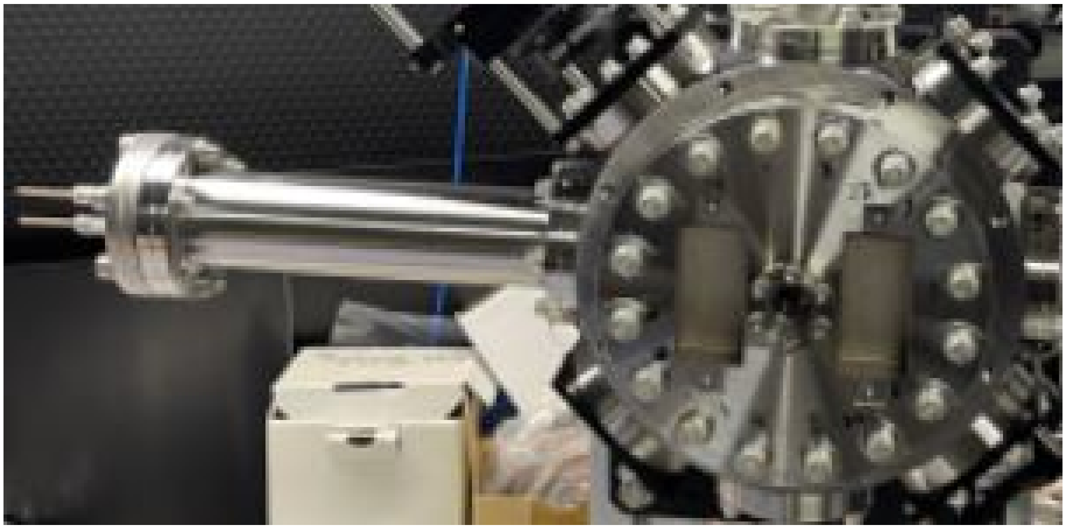

Figure 15: *Mount of the sealed oven alligned with the collimator on the viewport. The wires on the exterior allow heating of the oven.*

4.1.2 Current and heat requirements

In order to analyse the distribution of velocities for the calcium atoms, we need to explore further the vessel used in the calcium oven. The vessel is a product from Alfakuvo e.U. [11] the vessel design is shown in the graph below:

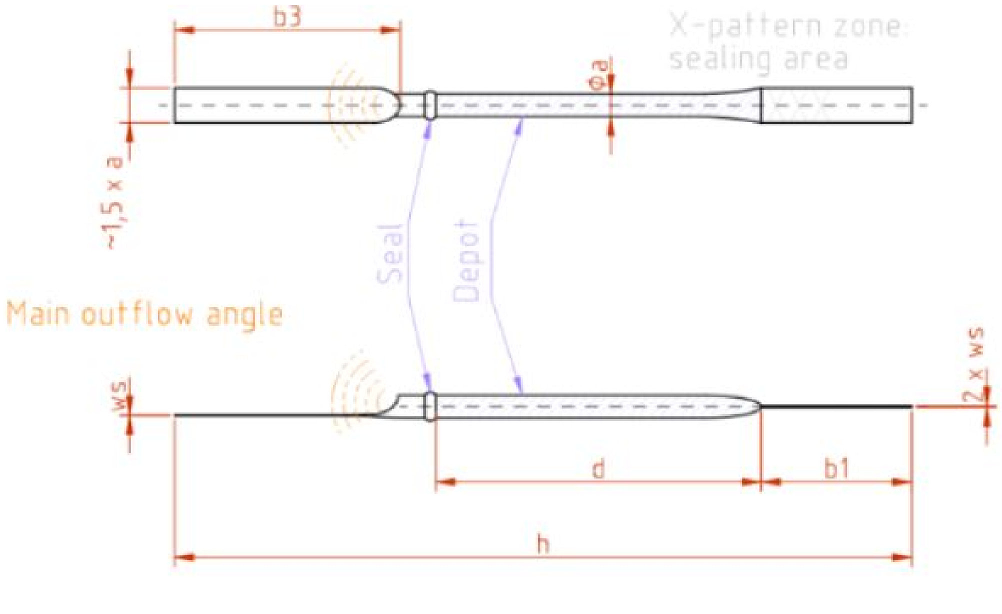

Figure 16: *design of the vessel carrying calcium particles from Alfakuvo*

At the outflow opening, the vessel is sealed by an Indium layer. It is melted to start liberating the particles. This temperature is called activation temperature. The evaporation temperature is the temperature at which the particles start evaporating out of the vessel. The values for these temperatures are shown below for various metals:

	ACTIVATION T_{MAX}	BAKE OUT T_{MAX}	EVAPORATION $T_{APPROX.}$	
PRESSURE MAX	1×10^{-3} Pa	1×10^{-3} Pa	1×10^{-4} Pa	1×10^{-6} Pa
ELEMENT / NOTE				
Al / pure	450-470 K	≤700 K	~1087 K	~958 K
Ba / pure	450-470 K	≤500 K	~647K	~566 K
Ca / pure	450-470 K	≤470 K	~626 K	~551 K

Figure 17: *Table of temperatures for metals from the Alfakuvo product description website*

We see that for Calcium, the activation is at 450 K, and the oven needs to be set for 30 minutes at that temperature to open the seal. Furthermore, we see the evaporation temperature decreases with the pressure at $10^{-6}Pa$ (10^{-8} mbar) it is at 551 K . In order to achieve such temperatures, we need to know the intensity of the current needed. From the datasheet in [11] we expect it to be at 6 A.

4.1.3 Distribution of velocities

In the analysis for the probability density distribution of velocities we set the temperature at 650 K as to be above the required temperature and we assume that after the evaporation temperature the particles act as an ideal gas, this gives the following distribution function from [13]:

$$p(v) = 4\pi \left(\frac{M}{2\pi R T}\right)^{3/2} v^2 \exp\left(-\frac{Mv^2}{2RT}\right) \tag{33}$$

Where M [kg/mol] is the molar mass of calcium , R [J/K.mol] is the gas constant T [K] the temperature and v [m/s] the velocity of particles. This results in the following distribution:

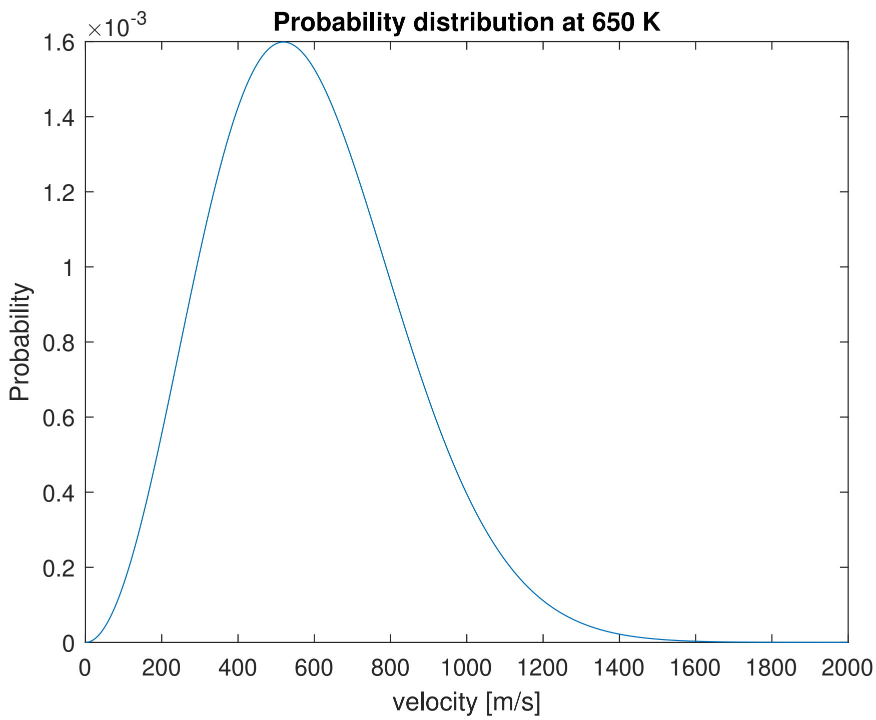

Figure 18: *Probability density distribution for the velocities of particles out of the oven at 650 k*

Furthermore, for the particle flux to enter the interaction region of the 2D-MOT, it must go through the opening of the collimator. The opening of the vessel is bigger than the opening in the collimator such that :

$$\frac{\mathrm{d}}{2} \leq \mathrm{r} \tag{34}$$

Since the solid angle distribution is considered uniform, we will assume the velocity distribution to be the same for particles entering the chamber.

4.2 Beam mounts and reflectors

We want to send beams for laser cooling perpendicular to each other and from both directions on each axis of the 2D MOT. Furthermore, the beams need to intersect at the centre of the chamber such that the intersection is in the path of the particle flux from the oven. The beams need to be precisely aligned and stable while entering. This is why we designed a mount for the beams to hold the fibre outputs toward a glass viewport directly. Symmetrically, reflective mirrors mounts are placed on the opposite side of the chamber from the beam .
The first step is to design a part that can hold the mount stably on the flange containing the glass viewport to . The design for this part is shown in the figure below:

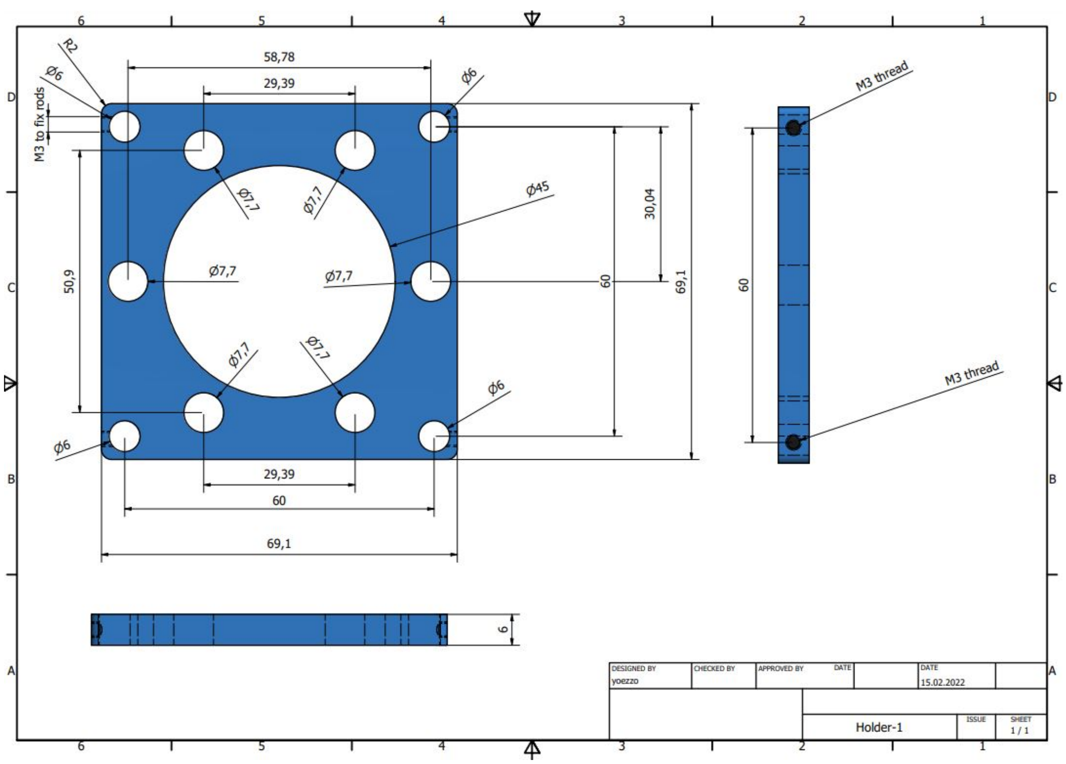

Figure 19: *connection to the viewport for the rest of the mount*

This connection needs to have an empty radius equal to the viewports'. Secondly, the six holes around fit the screws that attach the connector and the viewport to the chamber. Finally, the four holes will fit rods stabilised by m3 screws from the sides. This will allow us to attach the other components and precisely align them into the viewport.

4.2.1 Beam mounts

Specifically, the parts that are designed to mount the beam fit:

1. A collimator that is connected to the fibre from the laser setup
2. quarter-waveplate
3. focalising lens

The focalising lens allows maintaining the beam radius fixed in the chamber, so there is no loss of power when it is reflected. And the quarter-waveplate is used for a circular polarisation needed for the MOT beams. After connecting all these items via rods it give the following component for the beam mount:

Figure 20: *Mount for the MOT beams into the chamber*

4.2.2 Reflectors mount

The reflector mount consists of a mirror and a quarter-waveplate such that the back-reflected beam has the opposite circular polarization. One important note is that each of the two optics have different sizes and hence require different mounts that are attached to each other by another set of rods, as shown below:

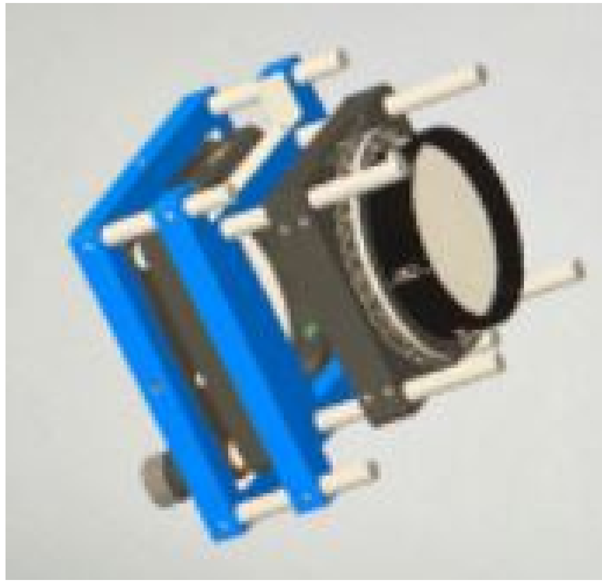

Figure 21: *Mount for the reflectors into the chamber*

4.3 Mount for the Zeeman slower beam

Unlike the standard MOT beam mounts, the Zeeman beam cannot be mounted directly in front of a viewport of the chamber. The beam is meant to oppose the particle flux direction to initially cool down the hot atoms from the oven to facilitate the trapping. Nevertheless, the flux incoming into the viewport will create a metallic deposit on it, making the efficiency of the Zeemann beam decrease over time and usage. Indeed, Particles can accumulate over time on the mirror, creating a reflecting metallic coating. This can decrease the reflectivity of the mirror over time but without completely obscuring the Zeeman slowing beam over time.

Hence, we designed a connection built into a T-shaped compartement, where a 45° inclined mirror is placed perpendicularly to the beam sending it into the Chamber. This will avoid the viewport to be in the flux path and with the tilted angle the mirror will avoid accumulation of the particles on it.
This why we custom made a mirror mount for the mirror to be set inside the T-shape connection presented in the figure below:

(a)

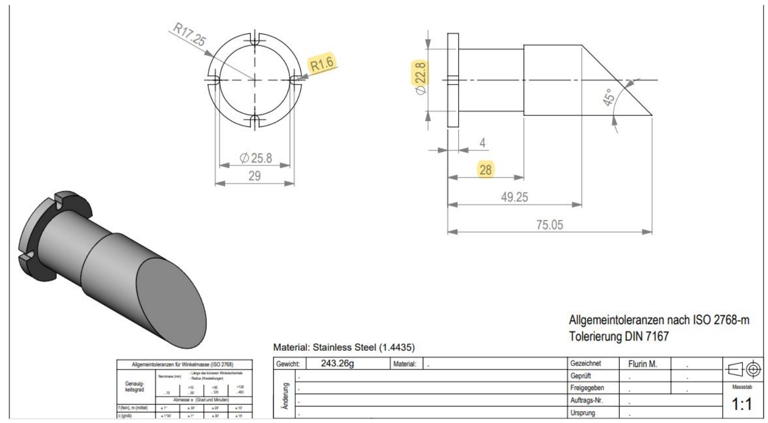

(b)

Figure 22: *Mirror handle final design(b) and mounting in a custom made flange to be put in the T-shaped connector(a)*

Furthermore, the mirror is placed on the handle with glue that hardens through heat. We used EPOXY H21D [14] to glue the mirror inside the vacuum chamber. The glue needs to be cured for one hour at 100 Celsius. It is advantageous as it can withstand temperatures to around 180 C°, which is necessary for all the chamber components as it will go through a bakeout at 150 C°.

Finally, we present the Zeeman connection mounted on the chamber in the figure below:

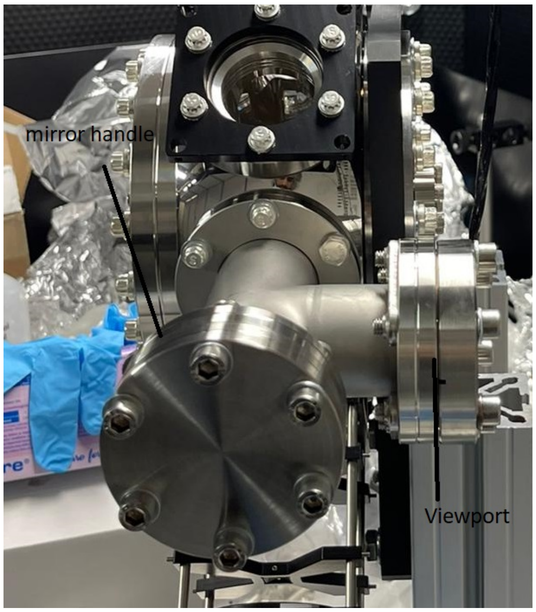

(a)

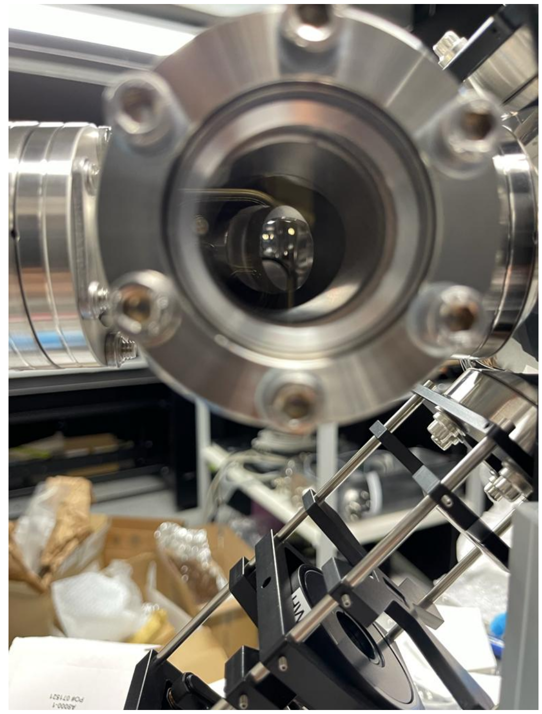

(b)

Figure 23: *Mounting of the Zeemann beam connection to the chamber.(a)Mirror flange view (b)Viewport view*

We can see in the middle of the mirror through the viewport the collimating disk of the oven, meaning the mirror is well placed.

4.4 Permanent magnets setup

The quadrupole like field is generated in our design by four sets of 9 permanent magnets, each with dimension 6mm x 15mm x 25mm and magnetisation M=$10^6 A/m$. Each two sets are on one side of the chamber, equally spaced from the centre. The main flanges enclosing the chamber are redesigned in order to fit those magnets as shown below:

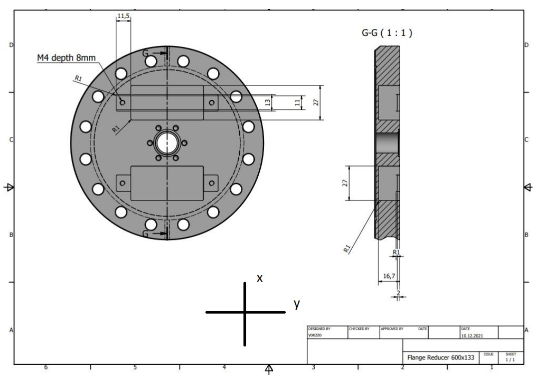

(a)

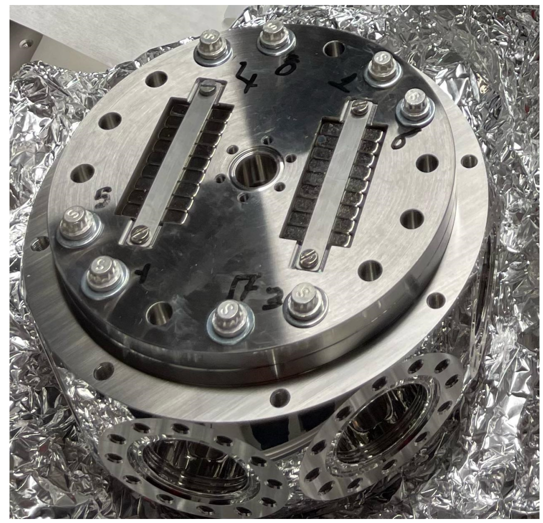

(b)

Figure 24: *Design of the modified flange of the chamber(a) Chamber with the magnets placed in the flange (b)*

The magnets are placed at 7 cm from the centre of the chamber. we take measurements using a Gaussmeter for inside the chamber to sample the magnetic field in the 2 axes, this gives the results in the figure below:

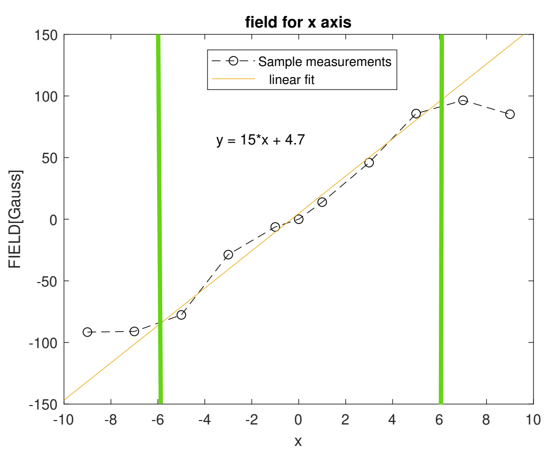

(a)

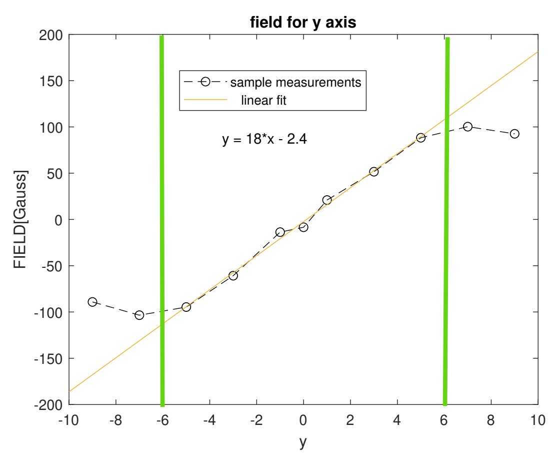

(b)

Figure 25: *Measurements of the magnetic field on the x-axis(a) and the y axis (b) the coordinates are from the centre of the chambre*

We note that on each axis, the absolute value of the field increases linearly between -6 and 6 cm. This is the shape we require for the desired magnetic effect to work properly in our MOT. We hence take a linear fit between these distances to determine the field gradient on each axis. For the x-axis, we have 15 G/cm and the y-axis 18G/cm

4.5 Pumping setup

The pumping setup we use is meant to achieve a UHV of $10^{-10} mbar$. Many preparations are required for such a high vacuum. Firstly all the components used in the setup need to go through a cleaning process. It requires using Acetone and isopropanol in a supersonic cleaner. Afterwards, all the parts connected to the chamber need to be tightly sealed and leak-free.

4.5.1 Leak test

Afterwards a leak test needs to be made for the assembled chamber. This is done by connecting the leak test setup shown below:

Figure 26: *Leak testing device connected to the chamber*

This device is connected to an ion pump mounted on the chamber. It first calibrates with the chamber to measure the leakage rate [mbar.l/s], then it uses a helium pistol to eject a small sample of helium. The pistol is pointed at each sealed port. If the device detects a variation in the leakage rate, this port is not properly sealed and will have leakage. There were signals for leaks in all the ports in our first test, which was highly unlikely. After exploring the issue, we found out that it was the ion pump in itself that was defective, and hence all the tests were invalid. It is important to note that if the connection to the pump or the pump in itself has leakage, the test will be invalid for the rest of the chamber.
After replacing the ion pump, the test shows that the chamber is leak free, the leak rate is at a stable value as shown below:

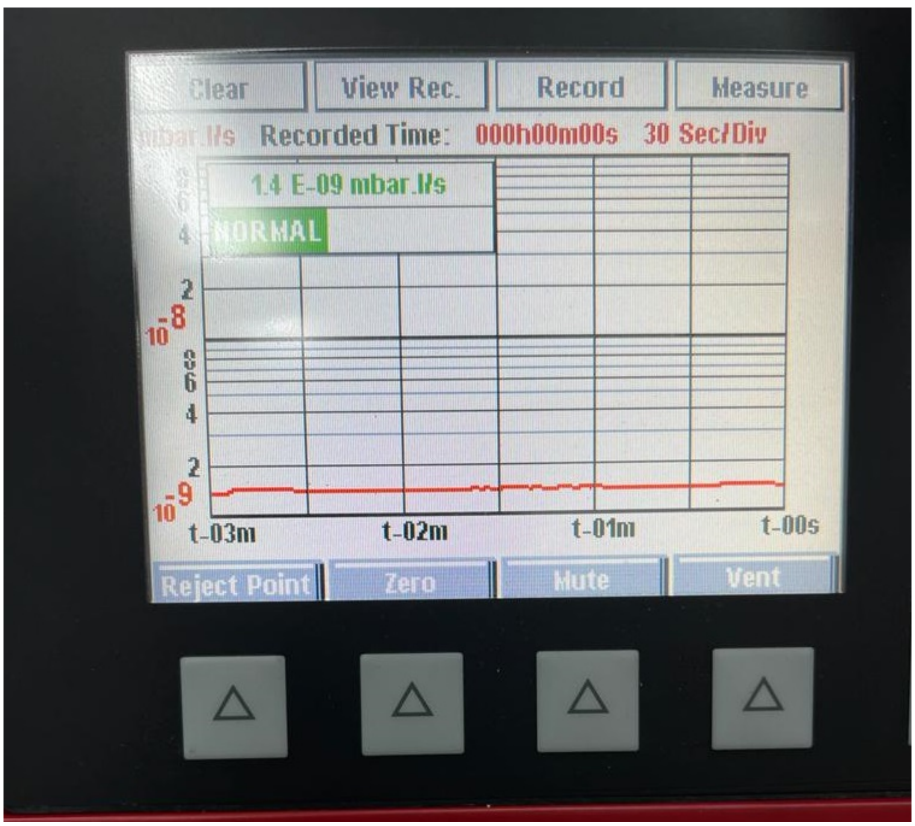

Figure 27: *Leakage rate stable all along the test after replacing the ion pump*

4.5.2 Baking of the chamber

Afterwards, the chamber is put in an oven and connected to a turbo molecular pump from the same connection used in the leak test. The pressure is brought down to

$10^{-}6mbar$, and we start the baking for five days at 150 $C°$. This is to help evaporate any residue oils or liquid in the chamber so the activated pumps can pump them. During this process, the pressure will slightly increase due to the temperature increase. The evolution of the baking and the pressure are shown in the figures below:

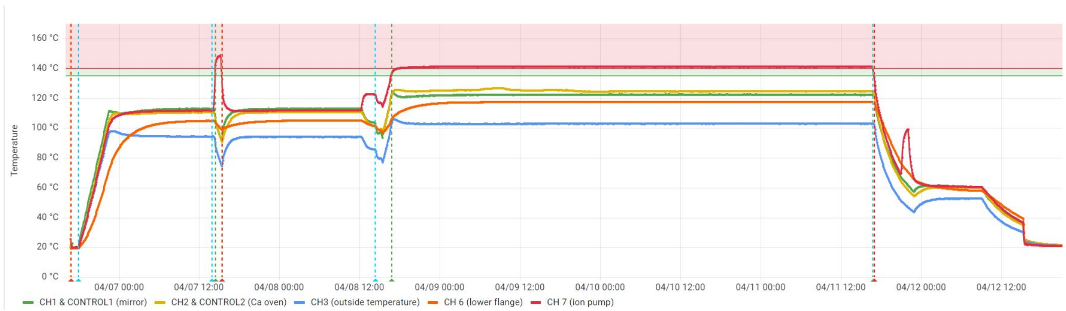

Figure 28: *Temperatures of the chamber measured through different channel. Depending on the position in the oven the temperatures are between 100 and 150 C]degree*

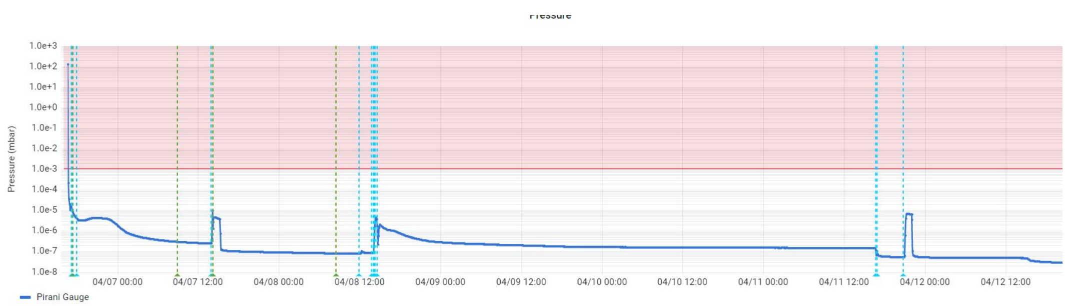

Figure 29: *Pressure measured for the duration of the pumping and baking*

We note a slight increase in pressure while the temperature of the chamber is rising, also three irregularities in both temperature and pressure during the baking of the oven. After finishing the baking process, the ion pump continues pumping, and we indeed reach a pressure of $5.7 * 10^{-10}$ mbar. This is the final step for making our setup ready to function. It is mounted on a Holder and will be connected to our laser setup:

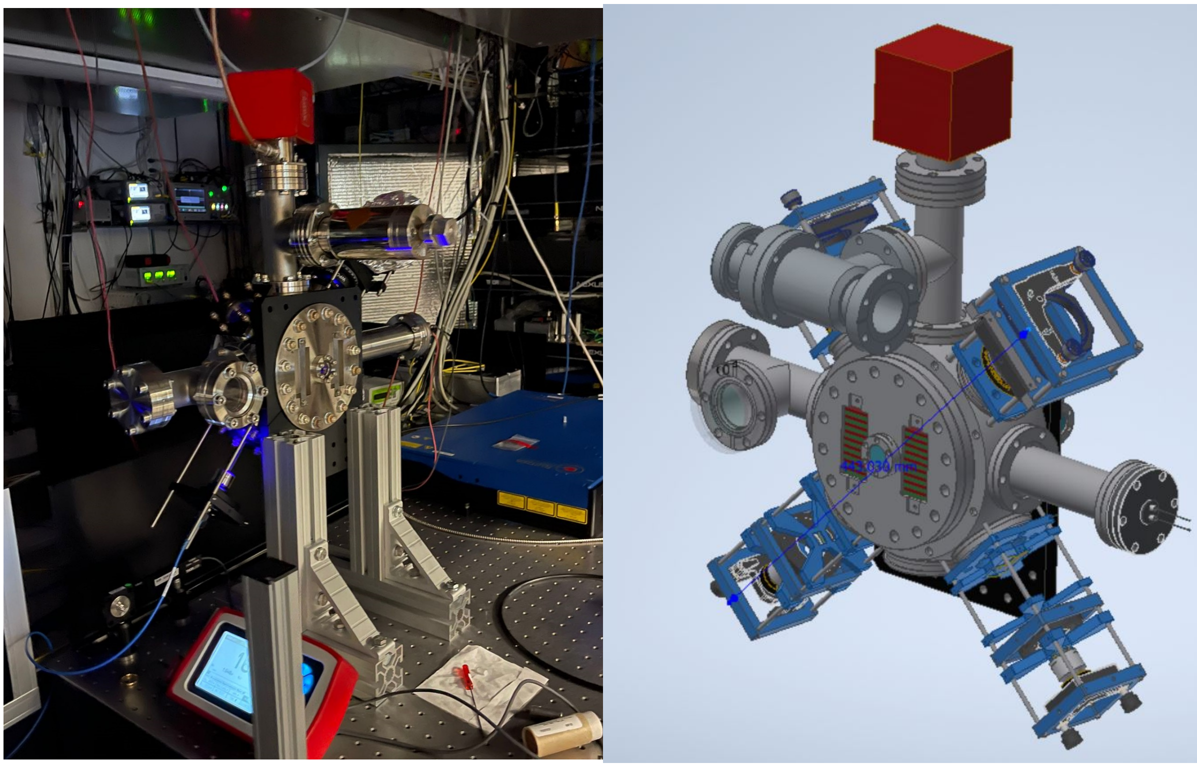

(a) (b)

Figure 30: *The asseblemd MOT chamber ready for use (a) Setup mounted in the lab (b) Adobe inventor assembly design*

5 Experimental results

In this chapter, we explore the experimental results obtained during the testing of our setup.

5.1 Laser setup results

First, in the table shown below we display the efficieny of the parts used in our laser setup:

part	theoretical value	experimental value
mirror	R>0.99	R=0.99
PBS/Half-waveplate	R>0.99(V), T>0.99(H)	R=0.99(V),T=0.99(H)
AOM (1st order)	T>0.90	T=0.80
AOM (Double passing)	T>0.81	T=0.64
Collimator Zeemann beam	T>0.90	T=0.79
Collimator laser source	T>0.90	T=0.83
Collimator MOT beam	T>0.90	T=0.85

Table 1: Theoretical efficiencies of the parts all obtained from Thorlabs and IntrAction Co. datasheets and experimental results

The half-waveplate has a 50/50 efficiency since we use one resulting beam for the Zeemann beam and the other for the MOT beam. We will take this into account and hence, we have a theoretical total Transmission(efficiency) for the Zeemann and MOT beams equal to:

$$\begin{aligned} \eta^{Zeemann}_{\text{theoretical}} &> 0.32 \\ \eta^{MOT}_{\text{theoretical}} &> 0.40 \\ \eta^{Total}_{\text{theoretical}} = \eta^{Zeemann}_{\text{theoretical}} + \eta^{MOT}_{\text{theoretical}} &> 0.72 \end{aligned} \tag{35}$$

Where here we consider the total transmission or effectiveness of our setup the total ratio of the collected beam amplitude at the end of our setup to the initial beam amplitude The corresponding theoretical values are:

$$\begin{aligned} \eta^{Zeemann}_{\text{experimental}} &= 0.20 \pm 0.005 \\ \eta^{MOT}_{\text{experimental}} &= 0.33 \pm 0.005 \\ \eta^{Total}_{\text{theoretical}} &= 0.52 \pm 0.005 \end{aligned} \tag{36}$$

The experimental and theoretical efficiency ratio is 72.2 %, which is good, but the Zeeman setup should be the main focus if a better experimental value is required.

The polarisation of the beam in the fibre after being optimised may have been shifted due to the movement of the fibre, which would affect the collimator efficiency from the laser source. Furthermore, the beam shape could be further improved as it was optimised by the naked eye. Furthermore, the beam blocker could be obstructing part of the diffracted beam invisible to the blind eye. Nevertheless, the ratio was considered acceptable to connect to the MOT chamber.

5.2 Chamber results

First, The pressure achieved after the baking and pumping process was found to be at $5.7.10^{-10} mbar$, which satisfies the requirement for an Ultra-High vacuum chamber.
Second, the magnetic field, as shown in Fig.30 shows a homogenous between the two magnets along each axis. The gradient value for the x-axis is 15 G/cm and the y-axis 18 g/cm, although these values contain uncertainty. This is attributed mostly to experimental error. An improvement would be to design a setup specifically made to measure magnetic fields inside the MOT chamber, where the control of the position and stability of the Gaussmeter could be precisely handled. These results show that the chamber satisfies the requirements needed to be used as a 2D-MOT.

6 Conclusion

During this master thesis project, we designed and built a 2D-MOT as a better candidate for loading calcium atoms. The mathematical description served as orientation for the requirements needed to be satisfied for our design to succeed. The laser setup was designed to be efficient and compact. It also allowed us to introduce novel software for RF generating devices like the TPI-synthesizer. We also note that the software allows the connection of multiple devices and the generation of their interface automatically. Which already prepares for expanding the laser setup if we need to control more beams in the future. The design proved to be experimentally viable with room for improvement.

Furthermore, the design of the chamber included a new oven setup and design along with the Zeeman beam facing the atom source in the chamber, which is an addition to the classical 2D-MOT. The experimental results for this design in terms of pressure proved efficient, and the magnetic field also proved to behave as required, with room for a better sampling method development.

The 2D-MOT viability as a loading method will further be explored by connecting to other devices, and it will be soon connected and used in a newly built setup for a cold atoms experiment in the TIQI group. A further benchmark will be to run numerical simulations of the atom's dynamics in our specific setup. These will be compared with experimental tests in order to better understand and optimize our design compared to more traditional atomic sources.

References

[1] *A Quantum wake up call for european CEOs ,McKinnsey Digital*
Link: `https://www.mckinsey.com/business-functions/mckinsey-digital/our-insights/a-quantum-wake-up-call-for-european-ceos: :text=A`

[2] Harold J. Metcalf, Peter van der Straten, and Peter van der Straten. Laser Cooling and Trapping (Graduate Texts in Contemporary Physics). Springer, 2001.

[3] P. D. Lett, W. D. Phillips, S. L. Rolston, C. E. Tanner, R. N. Watts, and C. I. Westbrook. Optical molasses. Journal of the Optical Society of America B, 6(11):2084, nov 1989

[4] Rev. Sci. Instrum. 84, 063102 (2013); https://doi.org/10.1063/1.4808375 Submitted: 03 April 2013 • Accepted: 20 May 2013 • Published Online: 07 June 2013

[5] D. R. Lide, editor, CRC handbook of chemistry and physics, CRC Press, 74th edition, 1995.

[6] Alcock, C. B., Itkin, V. P., and Horrigan, M. K., Canadian Metallurgical Quarterly, 23, 309, 1984.

[7] S. Hoekstra, A. K. Mollema, R. Morgenstern, H. W. Wilschut, and R. Hoekstra, Single-atom detection of calcium isotopes by atom-trap trace analysis, Phys. Rev. A 71, 023409 (2005)

[8] J. Grunert and A. Hemmerich, Optimizing the production of metastable Calcium atoms in a magneto-optic trap, Appl. Phys. B 64, 815 (2001).

[9] Thorlabs, Inc.
https://www.thorlabs.com/catalogpages/Obsolete/2020/CFC-2X-A.pdf

[10] Ian Norris. Laser cooling and trapping of neutral calcium atoms, 2009

[11] Alfavakuo Co. https://alfavakuo.eu/products/mvs/ABE

[12] Britannica, The Editors of Encyclopaedia. "Maxwell-Boltzmann distribution". Encyclopedia Britannica, 13 Apr. 2021, https://www.britannica.com/science/Maxwell-Boltzmann-distribution. Accessed 19 April 2022.

[13] *SAMUEL J. LING, TRUMAN STATE UNIVERSITY JEFF SANNY, LOYOLA MARYMOUNT UNIVERSITY WILLIAM MOEBS, FORMERLY OF LOYOLA MARYMOUNT UNIVERSITY,University physics. Volume 2*

[14] *Epotek , (https://www.epotek.com/docs/en/Datasheet/H21D.pdf)*

[15] *Review of Scientific Instruments 84, 063102 (2013); https://doi.org/10.1063/1.4808375*

[16] *http://laserscience.co.in/library/*

7 Appendix

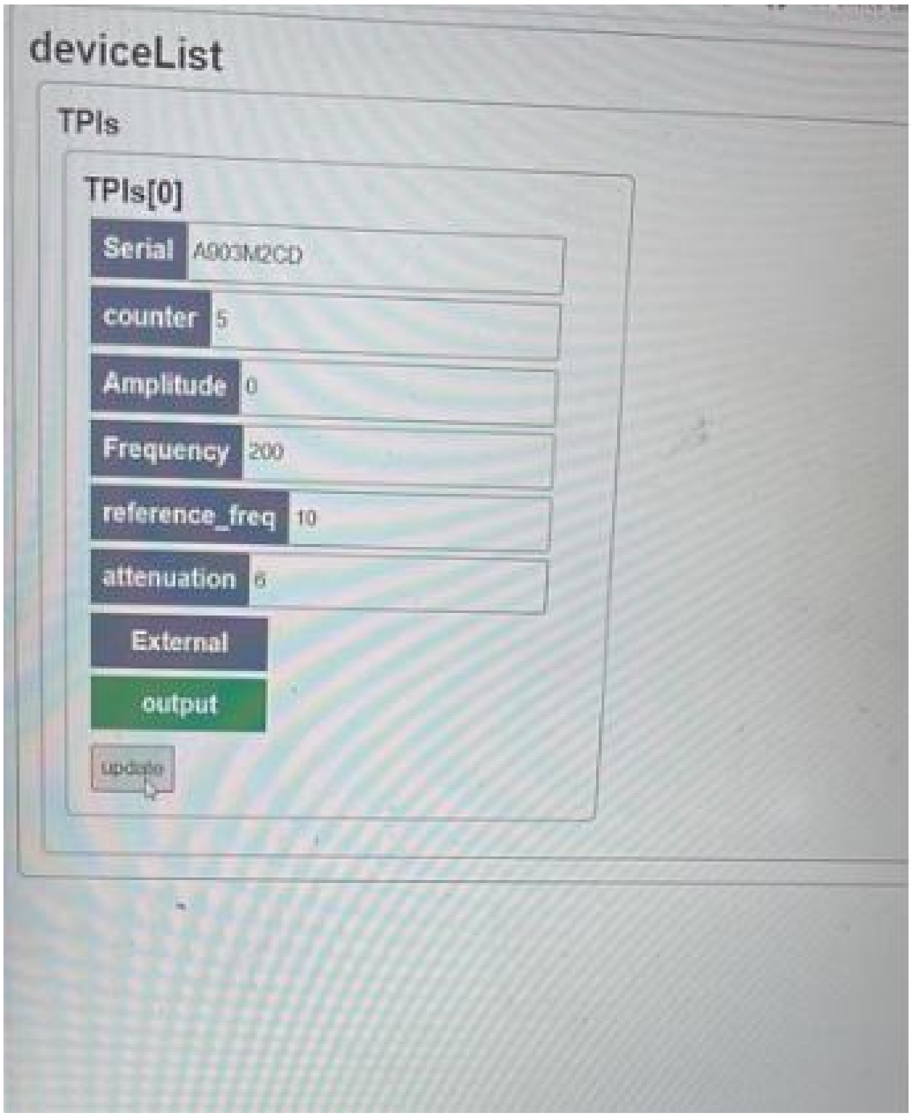

Figure 31: *Picture of the interface developped*

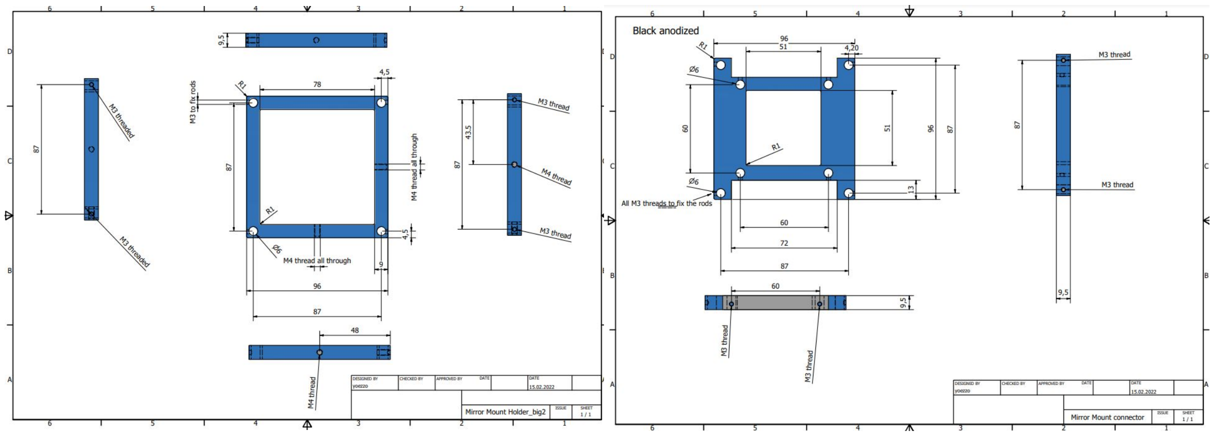

(a) (b)

Figure 32: *Different designs of other components used in the reflector mount*